Paull, C.K., Matsumoto, R., Wallace, P.J., and Dillon, W.P. (Eds.), 2000
Proceedings of the Ocean Drilling Program, Scientific Results, Vol. 164

30. ZONATION OF AUTHIGENIC CARBONATES WITHIN GAS HYDRATE–BEARING SEDIMENTARY SECTIONS ON THE BLAKE RIDGE: OFFSHORE SOUTHEASTERN NORTH AMERICA[1]

N.M. Rodriguez,[2,3] C.K. Paull,[2,4] and W.S. Borowski[2,3]

ABSTRACT

Authigenic carbonate mineral distributions are compared to pore-water geochemical profiles and used to evaluate diagenesis within sedimentary sections containing gas hydrates on the Blake Ridge (Ocean Drilling Program Sites 994, 995, and 997). Carbonate mineral distributions reveal three distinct diagenetic zones. (1) Carbonate minerals in the upper 20 m are primarily biogenic and show no evidence of diagenesis. The $\delta^{13}C$ and $\delta^{18}O$ values of calcite within this zone reflects marine carbonate (~0‰ Peedee belemnite [PDB]) formed in equilibrium with seawater. (2) Between 20 and 100 mbsf, calcite $\delta^{13}C$ values are distinctly negative (as low as –7.0‰), and authigenic dolomite is common (~2–40 wt%) with $\delta^{13}C$ values between –3.6‰ and 13.7‰. (3) Below 100 mbsf, dolomite abundance decreases to trace amounts, and disseminated siderite becomes the pervasive (~2–30 wt%) authigenic carbonate. Both siderite textures and stable isotope values indicate direct precipitation from pore fluids rather than dolomite replacement. The $\delta^{13}C$ and $\delta^{18}O$ values of siderite vary from 5.0‰ to 10.9‰ and 2.9‰ to 7.6‰, respectively.

Comparisons between the $\delta^{13}C$ profiles of dissolved inorganic carbon (DIC) and pore-water concentration gradients, with the $\delta^{13}C$ and $\delta^{18}O$ values of authigenic carbonates, delineate a distinct depth zonation for authigenic carbonate mineral formation. Coincidence of the most negative $\delta^{13}C_{DIC}$ values (≤–38‰) and negative $\delta^{13}C$ values of both calcite and dolomite, with pore-water alkalinity increases, sulfate depletion, and decreases in interstitial Ca^{2+} and Mg^{2+} concentrations at and below 20 mbsf, suggests that authigenic calcite and dolomite formation is initiated at the base of the sulfate reduction zone (~21 mbsf) and occurs down to ~100 mbsf.

Siderite formation apparently occurs between 120 and 450 mbsf; within, and above, the gas hydrate–bearing section of the sediment column (~200–450 mbsf). Siderite $\delta^{13}C$ and $\delta^{18}O$ values are nearly uniform from their shallowest occurrence to the bottom of the sedimentary section. However, present-day pore-water $^{13}C_{DIC}$ values are only similar to siderite $\delta^{13}C$ values between ~100 and 450 mbsf. Furthermore, calculated equilibrium $\delta^{18}O$ values of siderite match the measured $\delta^{18}O$ values of siderite between 120 and 450 mbsf. This interval is characterized by high alkalinity (40–120 mM) and low Ca^{2+} and Mg^{2+} concentrations, conditions that are consistent with siderite formation.

INTRODUCTION

One of the objectives of Ocean Drilling Program (ODP) Leg 164 was to establish the diagenetic effects associated with gas hydrate formation and decomposition. Because gas hydrates are not preserved in cores or in exposed outcrops, it is necessary to find diagenetic "fingerprints" (or proxies) to identify sediments that formerly contained gas hydrate. The physical and chemical characteristics of sedimentary sections currently containing gas hydrates provide distinct diagenetic environments that may promote the precipitation and preservation of carbonate minerals. Our study, therefore, focuses on the distribution of carbonate minerals in three gas hydrate–bearing sedimentary sections (Sites 994, 995, and 997) drilled during ODP Leg 164 on the crest of the Blake Ridge, offshore southeastern North America (Fig. 1).

Early diagenesis of marine sediment is commonly dominated by the oxidation of sedimentary organic matter (e.g. Berner, 1980). This degradation of organic matter takes place in a vertical succession of biogeochemical zones, with sulfate reduction, methane oxidation (anaerobic and aerobic methane oxidation), fermentation, and methanogenesis being the dominant diagenetic processes (Claypool and Kaplan, 1974; Berner, 1980; Reeburgh, 1983). In normal marine settings, sulfate is consumed by two principal diagenetic reactions: (1) microbially mediated oxidation of organic matter by sulfate reduction ($2CH_2O + SO_4^{2-} \rightarrow 2HCO_3^- + H_2S$), and (2) microbially mediated anaerobic methane oxidation ($CH_4 + SO_4^{2-} \rightarrow HCO_3^- + HS^- + H_2O$). These microbially mediated "net" reactions increase alkalinity (by production of bicarbonate [HCO_3^-]) and may stimulate carbonate

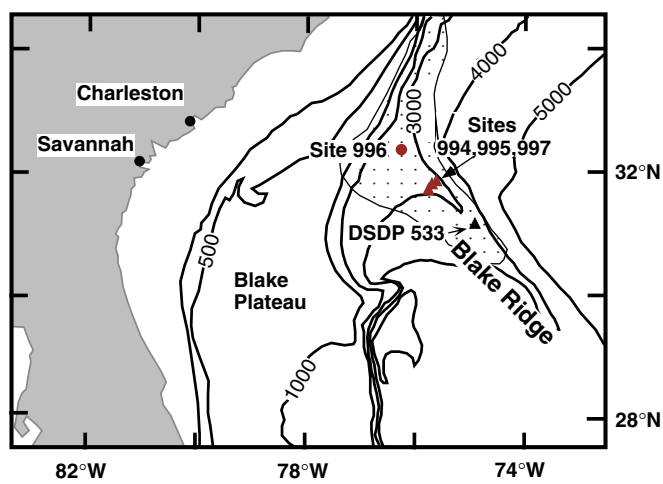

Figure 1. The location of Sites 994, 995, and 997 on the Blake Ridge, offshore southeastern North America, are shown. Bathymetry is in meters. The patterned area represents the region of the Carolina Rise and Blake Ridge where bottom-simulating reflectors, which indicate the presence of gas hydrates, are common (Dillon and Paull, 1983).

[1]Paull, C.K., Matsumoto, R., Wallace, P.J., and Dillon, W.P. (Eds.), 2000. *Proc. ODP, Sci. Results,* 164: College Station, TX (Ocean Drilling Program).

[2]Department of Geology, Mitchell Hall, University of North Carolina, Chapel Hill, NC 27599-3315, U.S.A.

[3]Present address: Exxon Exploration Company, Box 4778, Houston, TX 77210, U.S.A. Correspondence author: nmrodriguez@mindspring.com

[4]Present address: Monterey Bay Aquarium Research Institute, 7700 Sandholdt Road, Moss Landing, CA 95039-0628, U.S.A.

precipitation (Berner 1980; Baker and Burns, 1985). Furthermore, enhanced carbonate precipitation is predicted at the sulfate/methane boundary where focused anaerobic methane oxidation may produce sharp increases in pore-water alkalinity (Raiswell, 1988; Blair and Aller, 1995). Deeper in the sedimentary section, carbonate precipitation may be associated with methane production and gas hydrate formation (Claypool and Threlkeld, 1983; Kastner et al., 1990) and decomposition (Matsumoto, 1983; Matsumoto, 1989). The resulting carbonate minerals will reflect the isotopic signature of the dissolved inorganic carbon (DIC) pool in which they formed.

Authigenic carbonates, with carbon derived from methane, are known from numerous continental margin localities where methane-rich fluids seep to the sediment-water interface (e.g. Ritger et al., 1987; Hovland et al., 1987; Paull et al., 1992; Jørgensen, 1992; Roberts and Aharon, 1994; Paull et al., 1995; Nähr et al., Chap. 29, this volume). Modern methane-derived carbonates, however, have not been definitively identified in sedimentary sections where diffusive processes dominate.

Diagenetic dolomite is common in methane-bearing continental margin sediments (Baker and Burns, 1985; Kastner et al., 1990) where high alkalinities are common. The calcium and magnesium required for dolomite formation is generally provided by diffusion from overlying seawater and replacement of precursor calcite. Where calcium becomes limited, other carbonate minerals such as siderite or rhodochrosite will form (Baker and Burns, 1985; Compton and Seiver, 1986; Kastner et al., 1990). Furthermore, previous studies of the gas hydrate–bearing sediments on the Blake Ridge suggest that there is a link between formation of authigenic siderite and gas hydrate decomposition (Matsumoto, 1983, 1989).

Siderite ($FeCO_3$) formation is favored in anoxic environments where activities of dissolved sulfide are extremely low, and iron and bicarbonate activities are high (Taylor and Curtis, 1995); conditions that are present within the upper methanogenic and gas hydrate zones at the Blake Ridge (Paull, Matsumoto, Wallace, et al., 1996). Although a linkage between authigenic siderite formation and gas hydrate occurrence has been made only at the Blake Ridge (Lancelot and Ewing, 1972; Matsumoto, 1989), siderite occurrences are common in the methanogenic zone in other continental margin settings (Mozley and Carothers, 1992; Hicks, et al., 1996; Burns, 1997).

Changes in interstitial fluid compositions, particularly in dissolved Ca^{2+}, Mg^{2+}, and Sr^{2+} concentrations, are potentially useful indicators of carbonate diagenesis (Kastner et al., 1990). The principal sources for the solutes needed for diagenetic precipitation of carbonates include skeletal calcite (Ca^{2+}, Mg^{2+}, and HCO_3^-), seawater (Ca^{2+}, Mg^{2+}), clay minerals (Ca^{2+}, Mg^{2+}, and Fe^{2+}), the oxidation of sulfide minerals (Fe^{2+}), and organic matter degradation (HCO_3^-; Curtis and Coleman, 1986). Although the interstitial chemical environment controls carbonate diagenetic processes, the specific mechanism by which calcite, dolomite, or siderite precipitates (or dissolves) will produce predictable changes in interstitial Ca^{2+}, Mg^{2+}, and Sr^{2+} (Table 1).

The comparison of sediment properties such as mineralogy, texture, chemistry, and stable isotope measurements to current pore fluid chemistry in this study provides insight into the origin of carbonate minerals in the Blake Ridge sediments. Because drilling at Sites 994, 995, and 997 (700–750 mbsf; Paull, Matsumoto, Wallace, et al., 1996) penetrated the gas hydrate–bearing section of the sediment column (200–450 mbsf), well into the underlying gas hydrate–free sediments, the diagenetic environment within each of these diagenetic zones can be evaluated.

METHODS

Sediment samples collected from pore-water squeeze cakes and selected carbonate-rich horizons were washed with pH-10 distilled water (buffered with NH_4OH) to remove salts, freeze-dried, and powdered with an agate mortar and pestle for X-ray diffraction (XRD), percent $CaCO_3$, and stable isotope ($\delta^{18}O$ and $\delta^{13}C$) measurements. Bulk mineralogy was measured on randomly oriented samples by XRD, using monochromatic CuKα radiation on a Phillips Norelco 1720 at the University of North Carolina at Chapel Hill (UNC-CH). Scans were run from 5° to 70° 2θ, with a scan rate of 1.0° 2θ/min at 40kV/30mA. Each sample was spiked with an internal standard (20% potassium chloride [KCl]) to estimate the abundance of calcite, siderite, and dolomite. Weight percent of each mineral was determined by comparing the ratio of the reference peak (104) area (at 3.03Å, 2.89Å, and 2.79Å for calcite, dolomite, and siderite, respectively) to the reference peak (200) area of KCl (3.15Å) and comparing that ratio to calibration curves made for each mineral (Klug and Alexander, 1974). Total carbonate was measured by acid digestion and titration of evolved CO_2 using a Coulometrics Model 5011 CO_2 Coulometer at UNC-CH. To insure that all carbonate phases were digested, samples were acidified with 4-N HCL at 95°C for 10 min. CO_2-yield tests confirmed that this procedure removed all carbonate phases (aragonite, calcite, dolomite, and siderite). Selected subsamples were exam-

Table 1. Expected concentration changes in pore-fluid constituents due to carbonate diagenesis.

Carbonate reaction	Ca	Mg	Sr	Mg/Ca	Sr/Ca
Calcite precipitation: $Ca^{2+} + CO_3^{2-} \longrightarrow CaCO_3$	↓	—	↓	↑↑	↑
Calcite dissolution: $CaCO_3 + H^+ \longrightarrow Ca^{2+} + HCO_3^-$	↑	↑	↑	↓	↓
Calcite reprecipitation:	—	↑	↑	↑	↑
*Dolomite precipitation: $CaCO_3 + Mg^{2+} + 2HCO_3^- \longrightarrow CaMg(CO_3)_2 + CO_2 + H_2O$	—	↓	↑	↓	↑
Dolomite precipitation: $2CaCO_3 + Mg^{2+} \longrightarrow CaMg(CO_3)_2 + Ca^{2+}$	↑	↓	↓	↓	↓
*Dolomite precipitation: $Ca^{2+} + Mg^{2+} + 4HCO_3^- \longrightarrow CaMg(CO_3)_2 + 2CO_2 + 2H_2O$	↓	↓	↓	↑	↑
*Impure siderite precipitation: $2Fe^{2+} + Mg^{2+} + 2HCO_3^- \longrightarrow 2(Ca,Mg,Fe)CO_3^- + H_2$	↓	↓	↓	↓	↓
Impure siderite precipitation: $CaCO_3 + Fe^{2+} + Mg^{2+} \longrightarrow (Ca,Mg,Fe)CO_3 + Ca^{2+}$	↑	↓	↑	↓	↑
Siderite precipitation: $CaMg(CO_3)_2 + 2Fe^{2+} \longrightarrow 2FeCO_3 + Ca^{2+} + Mg^{2+}$	↑	↑	↑	↓	↓

Notes: ↑ = increases in concentration, ↓ = decreases in concentration, ↑↑ = considerable increases or decreases, — = no change. * = favored reaction for carbonate mineral precipitation at Sites 994, 995, and 997. Modified from Kastner et al. (1990).

ined with a Leica S440 Scanning Electron Microscope (SEM) and Energy Dispersive Spectrometer (EDS) at UNC-CH for qualitative evaluation of crystal habit and chemistry. Thin sections of epoxy-impregnated sediments were made and examined petrographically to evaluate the influence of diagenetic changes on sediment fabric.

Stable carbon and oxygen isotope measurements of the powdered samples involved digestion of carbonates under vacuum by selective extraction (Al-Aasm et al., 1990) in 100% phosphoric acid. All samples were placed in borosilicate vials and roasted under vacuum at 325°C for 1 hr to remove volatile organics. The samples were then placed in side-arm reaction vessels sitting in a heated water bath. Liberated CO_2 was cryogenically separated and then measured on a Finnigan Mat 251 Isotope Ratio Mass Spectrometer at North Carolina State University (NCSU), Raleigh, North Carolina, and on a VG-903 Isogas Source Stable Isotope Ratio Mass Spectrometer at Geochron Laboratories (Geochron) in Cambridge, Massachusetts. Evolved CO_2 was cryogenically separated at ~–130°C to prevent contamination with SO_2 produced during digestion of sulfide-bearing sediments (Des Marais, 1978).

The ^{13}C and ^{18}O values of calcite were measured at both NCSU and at Geochron Laboratories. At NCSU, calcite-digestion times were 10 min at 75°C. At Geochron, calcite digestion took place for 20 min at 50°C. Duplicate samples measured at both labs indicate that the data are internally consistent (± 0.2‰ for $\delta^{13}C$ and ± 0.4‰ for $\delta^{18}O$). Although there may be some dissolution of dolomite or siderite within the first 10 (at 75°C) or 20 (at 50°C) min of reaction with phosphoric acid, the extracted CO_2 is primarily that of calcite and should not affect the measurements appreciably.

The $\delta^{13}C$ and $\delta^{18}O$ values of dolomite and siderite were measured at Geochron Laboratories. After CO_2 generated by dissolution of calcite (20 min at 50°C) was withdrawn, the digestion vessels were again sealed and returned to the 50°C water bath, where digestion of the dolomite or siderite fraction of the sediment could proceed. A series of CO_2-yield/digestion-time experiments were run at Geochron (N.M. Rodriguez, unpubl. data) to estimate the amount of time required for dolomite and siderite digestion to go to completion. Complete digestion of dolomite and siderite in these experiments took place in ~12 and ~48 hr, respectively. Thus, samples containing primarily dolomite underwent continued digestion from 20 min to 24 hr. Samples containing primarily siderite underwent continued digestion from 20 min to 72 hr. Digestion residues from selected samples, which initially contained either siderite or dolomite, were evaluated by SEM to confirm that complete carbonate digestion occurred.

All stable isotopic measurements are reported with the δ notation, relative to Peedee belemnite (PDB). We have chosen not to apply specific phosphoric acid fractionation factors that account for the difference in fractionation between calcite and dolomite, or calcite and siderite (Table 2). Although specific phosphoric acid–liberated CO_2 fractionation factors exist (at a wide range of temperatures) for both stoichiometric siderite (Carothers et al., 1988) and dolomite (Rosenbaum and Sheppard, 1986), the scientific community currently lacks consensus on how to apply them to compositionally varied samples.

Table 2. Total carbonate content and isotopic composition of calcite, dolomite, and siderite in samples from Leg 164.

Core, section, interval (cm)	Depth (mbsf)	Total carbonate (wt%)	$\delta^{13}C$ ($CaCO_3$) (‰ PDB)	$\delta^{18}O$ ($CaCO_3$) (‰ PDB)	$\delta^{13}C$ (Dol/Sid) (‰ PDB)*	$\delta^{18}O$ (Dol/Sid) (‰ PDB)*	Mineral
164-994A-							
1H-1, 140-150	1.40	16	–0.19	–2.36	—	—	
1H-1, 140-150	1.40	16	–0.15	–2.00	—	—	
1H-1, 140-150	1.40	16	0.00	–1.20	–0.80	–5.10	Dolomite
1H-3, 140-150	4.40	19	–0.07	–0.32	—	—	
1H-3, 140-150	4.40	19	–0.05	–0.39	—	—	
1H-5, 140-150	7.40	19	0.19	–0.46	—	—	
1H-5, 140-150	7.40	19	0.12	–0.54	—	—	
2H-1, 140-150	9.30	46	0.60	–0.45	—	—	
2H-1, 140-150	9.30	46	0.60	0.10	0.70	–1.30	Dolomite
2H-3, 140-150	12.30	51	0.45	0.47	—	—	
2H-5, 140-150	15.30	40	0.66	0.52	—	—	
2H-5, 140-150	15.30	40	0.64	0.65	—	—	
3H-1, 140-150	18.80	26	0.21	0.36	—	—	
3H-2, 45-60	19.35	21	0.40	0.50	—	—	
3H-2, 80-95	19.70	25	–0.23	0.04	—	—	
3H-3, 10-25	20.50	24	–0.42	0.16	—	—	
3H-3, 80-95	21.20	26	–1.74	–0.29	—	—	
3H-3, 80-95	21.20	26	–2.37	0.12	—	—	
3H-3, 115-130	21.55	21	–1.43	–0.12	—	—	
3H-3, 140-150	21.80	23	–1.03	0.07	—	—	
3H-3, 140-150	21.80	23	–1.88	0.30	—	—	
3H-3, 140-150	21.80	23	–1.40	0.30	–0.40	–1.30	Dolomite
3H-5, 140-150	24.80	45	–3.56	1.12	—	—	
4H-2, 140-150	28.89	38	–3.90	1.21	—	—	
4H-2, 140-150	28.89	38	–3.97	1.33	—	—	
4H-2, 140-150	28.89	38	–2.90	1.40	–10.30	2.17	Dolomite
4H-4, 140-150	31.89	19	–1.99	0.04	—	—	
4H-6, 140-150	34.89	44	–4.58	2.13	—	—	
4H-6, 140-150	34.89	44	–4.60	2.02	—	—	
4H-6, 140-150	34.89	44	–3.30	2.17	–13.30	4.99	Dolomite
164-994C-							
5H-5, 145-150	40.35	27	–1.01	0.17	—	—	
5H-6, 90-91	41.30	68	–6.30	4.50	–13.70	4.00	Dolomite
5H-6, 90-92	41.30	67	–7.34	3.74	—	—	
6H-4, 145-150	48.05	16	–0.43	–0.25	—	—	
7H-4, 145-150	57.85	19	–0.41	0.10	—	—	
7H-4, 145-150	57.85	19	–0.38	0.19	—	—	
10H-1, 121-123	73.12	72	–0.43	3.84	—	—	
10H-1, 121-123	73.12	69	0.70	4.00	–3.60	4.60	Dolomite
10H-6, 102-103	80.42	59	–2.90	2.40	–8.50	2.90	Dolomite
12H-2, 140-150	93.80	21	0.04	0.31	—	—	
12H-2, 140-150	93.80	21	0.08	0.65	—	—	
17H-3, 140-150	142.80	11	–0.35	0.39	—	—	
30X-2, 140-150	244.60	14	0.42	–0.04	—	—	
30X-2, 140-150	244.60	14	0.30	0.30	5.00	4.00	Siderite
164-994D-							
4X–1, 51-53	261.52	23	0.70	0.50	4.90	4.20	Siderite

Table 2 (continued).

Core, section, interval (cm)	Depth (mbsf)	Total carbonate (wt%)	$\delta^{13}C$ ($CaCO_3$) (‰ PDB)	$\delta^{18}O$ ($CaCO_3$) (‰ PDB)	$\delta^{13}C$ (Dol/Sid) (‰ PDB)*	$\delta^{18}O$ (Dol/Sid) (‰ PDB)*	Mineral
164-994C-							
44X–1, 135-150	368.15	15	0.65	0.45	—	—	
54X-3, 140-150	439.50	19	0.55	0.30	—	—	
54X-3, 140-150	439.50	19	0.40	0.30	4.20	2.90	Siderite
75X-4, 135-150	613.05	10	0.80	0.66	—	—	
78X–1, 62-63	636.82	42	–1.90	1.60	8.60	6.60	Siderite
78X-4, 120-122	641.43	16	–4.40	1.50	6.60	5.00	Siderite
83X-3, 57-59	687.26	20	–4.00	1.20	8.00	5.60	Siderite
164-995B-							
1H-1, 38-48	0.38	46	1.59	–0.44	—	—	
1H-1, 38-48	0.38	46	1.57	–0.50	—	—	
1H-3, 108-118	4.08	19	0.40	–0.86	—	—	
1H-3, 108-118	4.08	19	0.30	0.90	—	—	
1H-5, 140-150	7.40	47	0.64	0.50	—	—	
1H-5, 140-150	7.40	47	0.55	0.05	—	—	
164-995A-							
3H-1, 150-155	12.73	23	–0.29	0.06	—	—	
3H-1, 150-155	12.73	23	–0.24	–0.15	—	—	
3H-3, 145-150	15.75	25	0.41	–0.27	—	—	
164-995B-							
2H-1, 140-150	17.40	19	0.73	0.16	—	—	
2H-2, 140-150	18.90	23	–0.40	0.61	—	—	
2H-2, 140-150	18.90	23	–0.40	0.25	—	—	
2H-3, 140-150	20.40	19	–0.30	0.20	—	—	
2H-4, 10-20	20.60	19	0.10	–1.69	—	—	
2H-4, 30-40	20.80	18	0.04	–0.14	—	—	
2H-4, 72-82	21.22	25	–0.07	–0.93	—	—	
2H-4, 92-102	21.42	25	–0.09	–0.22	—	—	
2H-4, 92-102	21.42	25	–0.30	0.50	—	—	
2H-4, 122-132	21.72	18	0.37	0.51	—	—	
2H-4, 140-150	21.90	33	–0.26	0.62	—	—	
2H-5, 140-150	23.40	37	–1.07	0.32	—	—	
2H-5, 140-150	23.40	37	–0.98	0.39	—	—	
164-995A-							
5H-5, 145-150	37.65	6	0.01	–0.03	—	—	
6H-5, 140-150	47.10	24	–0.18	0.35	—	—	
6H-6, 83-85	48.04	72	–3.50	3.30	–9.20	3.70	Dolomite
13H-5, 140-150	105.10	26	0.72	0.54	—	—	
13H-5, 140-150	105.10	26	0.80	0.60	–0.30	1.00	Dolomite
13H-5, 140-150	105.20	26	0.20	0.70	—	—	
17H-5,1 40-150	143.10	18	–0.30	0.88	5.70	5.60	Siderite
17H-5, 140-150	143.10	18	–0.40	0.80	5.50	5.40	Siderite
24X-1, 135-150	195.35	11	0.65	0.24	—	—	
24X-1, 135-150	195.35	11	0.40	0.30	6.60	4.00	Siderite
26X-1, 24-26	214.08	6	0.20	–0.30	6.70	4.40	Siderite
31X-6, 38-40	260.12	14	–0.10	0.50	6.80	5.00	Siderite
36P-1, 9-24	300.39	13	0.30	0.40	5.00	4.20	Siderite
42X-1, 130-150	349.90	18	–0.18	0.35	—	—	
42X-1, 130-150	349.90	18	–0.11	0.49	—	—	
42X-3, 103-104	352.63	14	–0.10	–0.10	6.40	5.10	Siderite
46X-3, 140-150	382.39	12	–0.60	0.40	4.00	3.70	Siderite
49X-4, 140-150	403.60	19	0.40	0.50	3.70	3.30	Siderite
55X-1, 130-150	446.20	19	0.88	0.72	—	—	
55X-1, 130-150	446.20	19	0.60	0.60	6.60	4.70	Siderite
61X-6, 9-39	500.34	12	0.60	0.40	6.50	4.30	Siderite
71X-6, 141-142	588.75	36	–3.20	2.50	9.30	6.30	Siderite
71X-6, 141-143	588.76	26	–1.90	2.90	9.40	3.90	Siderite
81X-5, 95-96	682.66	23	–3.80	1.30	8.70	6.00	Siderite
83X-7, 0-20	703.80	11	–0.03	0.63	—	—	
83X-7, 0-20	703.80	11	–0.77	0.20	—	—	
164-997A-							
5H-CC, 20-21	41.19	70	–6.50	5.60	–11.90	5.70	Dolomite
8H-3, 15-16	56.05	67	–0.80	6.70	–10.00	7.10	Dolomite
21X-2, 140-150	169.80	10	0.60	0.50	6.50	2.40	Siderite
26X-2, 50-52	205.41	11	0.40	0.50	7.20	6.20	Siderite
26X-2, 51-52	205.42	36	0.60	3.10	8.30	7.60	Siderite
164-997B-							
2X-2, 49-50	330.10	20	0.40	0.40	7.80	4.90	Siderite
8X-3, 141-143	447.42	17	–0.50	0.40	9.10	5.70	Siderite
20X-3, 125-150	543.45	10	0.40	0.30	8.90	3.60	Siderite
23X-3,120-121	562.60	18	–1.80	1.00	10.90	6.00	Siderite
33X-2, 109-111	638.06	15	–3.60	1.10	8.00	5.20	Siderite
33X-2, 110-111	638.07	44	–10.70	2.80	8.50	5.70	Siderite
46X-3, 120-121	734.44	36	–2.80	2.00	6.60	6.20	Siderite

Note: * = no dolomite- or siderite-specific phosphoric-acid correction factors have been applied to these $\delta^{18}O$ values.

Fractionation factors for "impure" dolomites and siderite are uncertain due to the relationship between the chemical composition of a carbonate mineral and its phosphoric acid–liberated CO_2 fractionation factor (Land, 1980; Rosenbaum and Sheppard, 1986).

Pore-water samples were obtained by routine shipboard squeezing of whole-round sediment samples shortly after core recovery (Manheim and Sayles, 1974). Interstitial Ca^{2+} and Mg^{2+} concentrations, Sr^{2+} concentrations, and total alkalinity were measured by ion chromatography, atomic absorption spectrometry, and titration respectively (Gieskes et al., 1991; Paull, Matsumoto, Wallace, et al., 1996). Aliquots of pore water were flame sealed in glass ampoules and stored for shore-based analysis. Pore-water samples were analyzed for $\delta^{13}C$ of DIC by acidification with 33% H_3PO_4 to liberate CO_2, which was cryogenically separated and analyzed on a Delta E mass spectrometer at NCSU (Borowski et al., Chap. 9, this volume; Paull et al., Chap. 7, this volume).

Age estimates for Sites 994, 995, and 997 are based upon detailed nannofossil datums for each site (Paull, Matsumoto, Wallace, et al., 1996) and reported relative to the late Neogene timescale of Shackleton et al. (1995). Host sediment ages are then estimated by assuming a constant sedimentation rate between nannofossil datums.

RESULTS

Relevant Shipboard Data

Pore-water chemistry, sediment mineralogy, porosity, and biostratigraphy are similar at Sites 994, 995, and 997. Therefore, all three sites are presented together as one composite section. These sedimentary sections are characterized by fairly homogeneous nannofossil-rich clays and claystones, with overall carbonate content and porosity decreasing with depth. Throughout the sedimentary section, clay minerals, calcite, and quartz are the dominant mineral components, whereas feldspar minerals and pyrite generally only make up a few percent of the bulk mineralogy. As discussed below, dolomite and siderite abundance are depth stratified.

Shipboard measurements (Paull, Matsumoto, Wallace, et al., 1996) of pore-water Ca^{2+}, Mg^{2+}, and Sr^{2+} concentrations reveal a dramatic decrease in the upper 40 mbsf, whereas alkalinity increases significantly over the same interval (Fig. 2). Sr^{2+} concentrations and Sr/Cl ratios fall below seawater values between 100 and 450 mbsf. This zone of low Sr^{2+} concentration overlaps the sediment zone (~200–450 mbsf) where gas hydrates were detected at these sites (Paull, Matsumoto, Wallace, et al., 1996). There is also a gradual decrease in Mg^{2+} concentrations within this sediment zone. Beneath the base of gas hydrate stability (~450 mbsf), pore-water Ca^{2+} and Sr^{2+} concentrations increase, and alkalinity decreases.

Measurements of alkalinity reach a maximum (as high as 120 mM at ~300 mbsf) within the gas hydrate–bearing section of the sediment column and decrease to values around 30 mM at the base of the hole (Fig. 2). The extremely high alkalinities observed in the gas hydrate–bearing section of the sediment column, and subsequent decrease, may be an artifact of outgassing from sediments containing gas hydrates (Paull et al., Chap. 7, this volume).

Distribution of Carbonate Minerals

Calcite is present throughout the sedimentary section and ranges from approximately 5 to 60 wt% (Paull, Matsumoto, Wallace, et al., 1996). Calcite abundance is greatest in the upper 100 m (average 20 ± 11 wt%) of the sedimentary section and generally decreases below 100 mbsf to the bottom of the hole (average 11 ± 3 wt%). Evaluation of smear slides indicates that the calcite in these sedimentary sections is generally of biogenic origin, consisting primarily of coccoliths and foraminifers (Fig. 3A).

Authigenic carbonates in the sedimentary section exhibit a clear vertical zonation (Table 3; Fig. 4). Dolomite is only present in significant quantities above 100 mbsf, whereas siderite is present in all samples below 150 mbsf. Although trace amounts (<2%) of dolomite are generally present in the upper 20 m, dolomite occurs in significant amounts (up to ~40 wt%) between 20 and 80 mbsf. Routine core descriptions, along with evaluation of both sediment smear slides (both shipboard and postcruise) and thin sections, indicate that dolomite is present as discrete microcrystalline nodules (up to 6 cm in diameter) and disseminated throughout the sedimentary section between 20 and 100 mbsf. SEM observations indicate that both disseminated and nodular dolomite consists of euhedral rhombs (Fig. 3B), and is thus dominantly authigenic. Between 100 and 120 mbsf, dolomite abundance decreases to trace amounts and is absent below 140 mbsf.

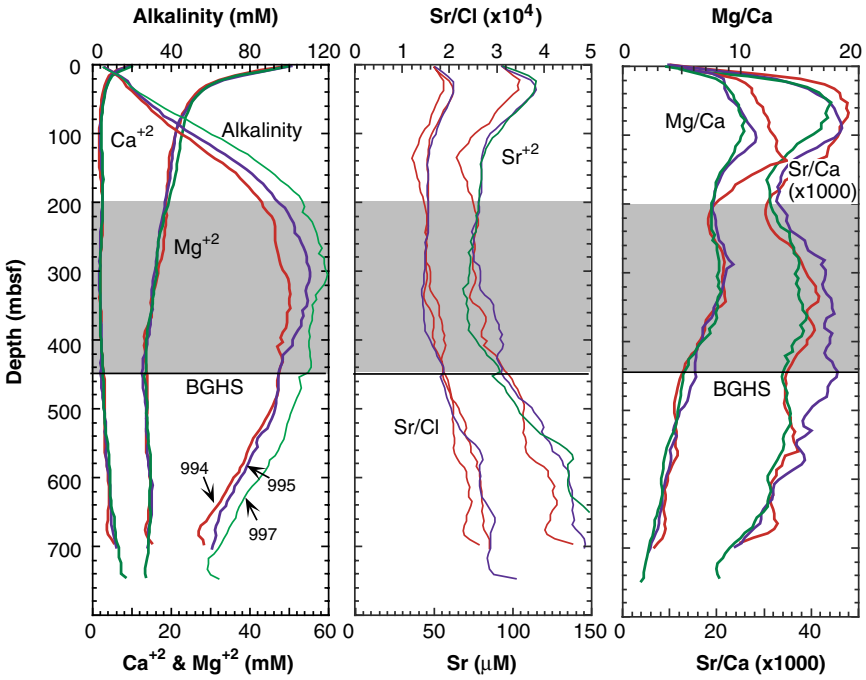

Figure 2. Variations of selected pore-water chemical constituents (Ca^{2+}, Mg^{2+}, and Sr^{2+} concentrations; total alkalinity; and Sr/Cl, Sr/Ca, and Mg/Ca ratios) vs. depth from Sites 994, 995, and 997 are shown (Paull, Matsumoto, Wallace, et al., 1996). Shaded area denotes region of sediment column where gas hydrates detected. BGHS represents the base of gas hydrate stability.

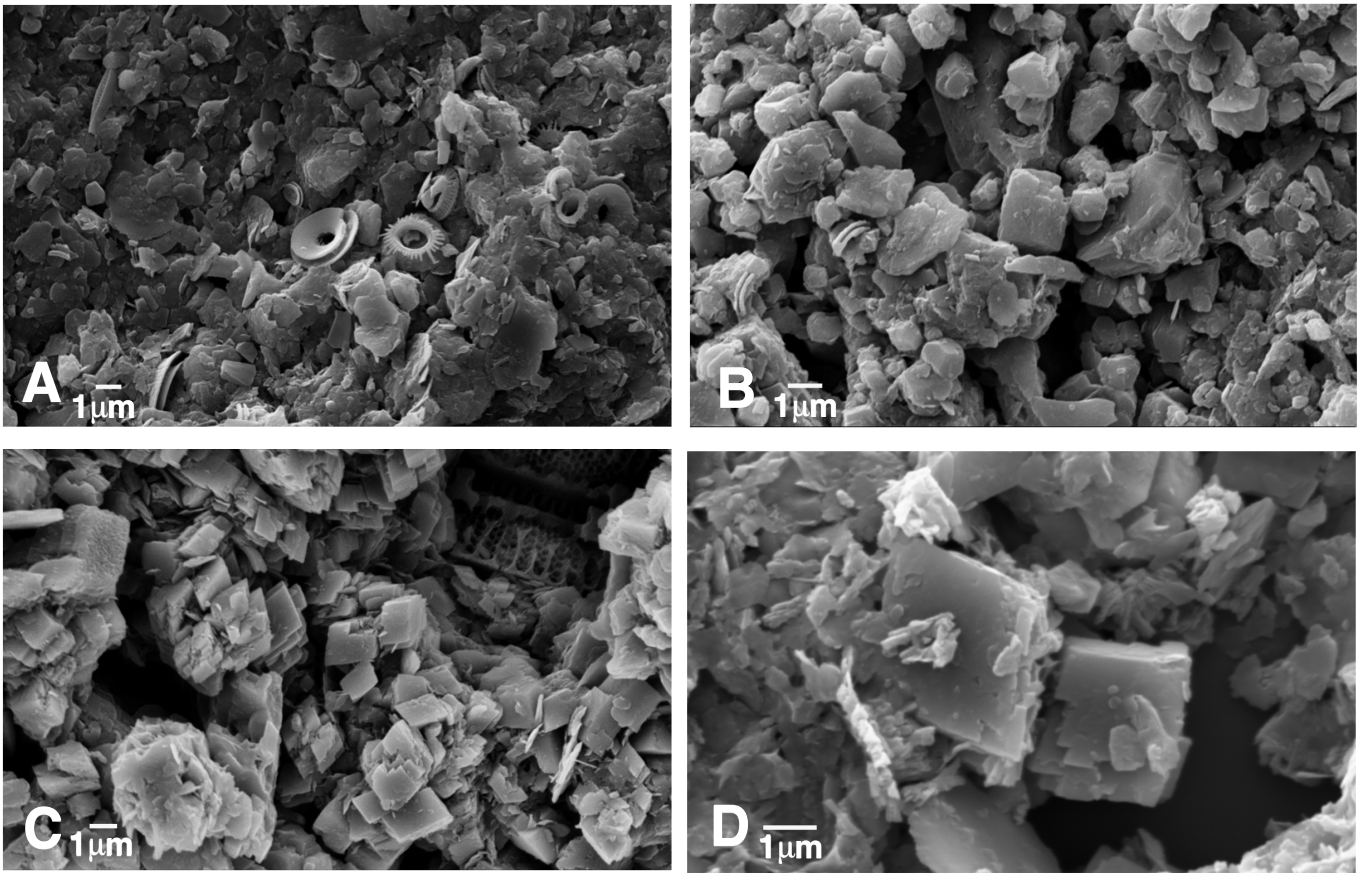

Figure 3. SEM photomicrographs show sediments from three different diagenetic zones. **A.** Sample 164-995A-2H-3, 69–71 cm (6 mbsf), illustrates typical hemipelagic sediment in the upper 20 mbsf lacking obvious authigenic crystals. **B.** Sample 164-995A-6H-6, 83–85 cm (48 mbsf), shows microcrystalline euhedral dolomite rhombs, ~2 μm in size, typical of the sediments recovered between 20 and 80 mbsf. The euhedral shape of the crystals implies an authigenic origin. **C**. Sample 164-997A-26X-2, 51–52 cm (205 mbsf), from the top of the gas hydrate zone, exhibits clusters of euhedral siderite rhombs, ~2 μm in size. **D.** Sample 164-997B-33X-2, 110–111cm, 638 mbsf; exhibits euhedral siderite rhombs.

On the basis of both smear-slide observations and XRD results, siderite occurrence is sporadic between 100 and 120 mbsf. Below 120 mbsf, disseminated siderite occupies 2–4 wt% of the sediment, or is present as small (<0.5-cm diameter) microcrystalline nodules of siderite occupying up to ~30 wt% (Table 3; Fig. 4; Paull, Matsumoto, Wallace, et al., 1996). As with dolomite, petrographic and SEM observations indicate that both disseminated and nodular siderite contains euhedral, microcrystalline rhombs, and is thus authigenic in origin. Qualitative EDS analysis of siderite throughout the sedimentary section indicates that the siderite contains approximately 10% Ca, 30% Mg, and 60% Fe.

Stable Isotope Studies

Calcite $\delta^{13}C$ values from Sites 994, 995, and 997 range from 1.6‰ to –10.7‰ with a mean value of –0.83‰ ± 1.97‰ and a median value of –0.15‰ (n = 125). Calcite $\delta^{18}O$ values range from +6.0‰ to –2.0‰ with a mean value of 0.69‰ ± 1.34‰ and a median of 0.4‰ (n = 125). The calcite ^{13}C and $\delta^{18}O$ values (Fig. 5) generally reflect isotopic values typical of biogenic carbonates in equilibrium with seawater (both $\delta^{13}C$ and $\delta^{18}0$ of ~0.2‰). However, between 20 and 100 mbsf, $\delta^{13}C$ values of calcite are typically more negative (down to –7‰, with a mean of –1.66‰ [n = 44]), and $\delta^{18}O$ values become positive (up to 6‰, with a mean of 1.13‰ ± 1.78‰ [n = 44]). In addition, calcite associated with some siderite nodules deep in the sedimentary section (~600 mbsf) also exhibit negative $\delta^{13}C$ values (Table 2; Fig. 5A). In these samples, calcite with negative $\delta^{13}C$ values tends to have corresponding positive $\delta^{18}O$ values (Fig. 6).

The $\delta^{13}C$ values for dolomite range from approximately –14‰ to 0‰ with a mean of –6.2‰ ± 5.4‰ (n = 14). The $\delta^{18}O$ values of dolomite range from 5.1‰ to +7.1‰ with a mean of 2.37‰ ± 3.3‰. Only dolomites found within the upper 22 mbsf have negative $\delta^{18}O$ values; dolomites found between 22 and 100 mbsf range from 1.0‰ to 7.1‰ (Table 2; Figs. 5–6).

The $\delta^{13}C$ values of siderite range from approximately 4‰ to 11‰ with a mean of 6.9‰ ± 1.8‰ (n = 31). Siderite $\delta^{18}O$ values range from 2.9‰ to 7.6‰ with a mean of 4.9‰ ± 1.2‰ (Table 2; Figs. 5–6).

The $\delta^{13}C$ values of pore-water DIC range from 10‰ at 144 mbsf to –38‰ at 20.4 mbsf, and the $\delta^{13}C$ values of CO_2 (gas) range from 1.1‰ at 141 mbsf to –32.7‰ at 48 mbsf. From a maximum at ~140 mbsf, pore-water DIC and $CO_{2\,(gas)}$ $\delta^{13}C$ values decrease to ~–4‰ and –18‰, respectively (Paull et al., Chap. 7, this volume; Fig. 7).

DISCUSSION

Diagenetic Zonation of Carbonate Minerals

Evaluation of pore-fluid chemistry and the mineralogical and isotopic composition of carbonate minerals at Sites 994, 995, and 997 reveal three distinct diagenetic zones. (1) In the upper 20 m, carbonate minerals show no evidence of a diagenetic overprint. (2) Between 20 and 80 mbsf, authigenic dolomite and calcite is common. (3) At

Table 3. Relative abundance of carbonate minerals in Leg 164 samples as determined by postcruise X-ray diffraction.

Core, section, interval (cm)	Depth (mbsf)	XRD Calcite (wt%)	XRD Dolomite (wt%)	XRD Siderite (wt%)
164-994A-				
1H-1, 140-150	1.40	10	4	0
2H-1, 140-150	9.30	45	8	0
2H-5, 140-150	15.30	38	2	0
3H-2, 45-60	19.35	15	1	0
3H-3, 140-150	21.80	23	3	0
3H-5, 140-150	24.80	28	3	0
4H-2, 140-150	28.89	20	5	0
4H-6, 140-150	34.89	27	7	0
164-994C-				
5H-6, 90-91	41.30	12	32	0
5H-6, 90-92	41.31	13	27	0
10H-1, 121-123	73.12	13	43	0
10H-6, 102-103	80.42	23	37	0
12H-2, 140-150	93.80	15	0	2
12H-5, 124-125	98.14	26	14	0
17H-3,140-150	142.80	10	0	0
30X-2, 140-150	244.60	11	0	1
164-994D-				
4X-1, 51-53	261.52	17	0	2
4X-1, 51-53	261.52	18	0	2
164-994C-				
44X-1, 135-150	368.15	13	0	2
52X-2, 21-23	426.22	14	0	2
54X-3, 140-150	439.50	19	0	2
75X-4, 24-26	612.00	15	0	2
75X-4, 135-150	613.05	8	0	2
78X-1, 60-62	636.81	11	0	5
78X-1, 62-63	636.82	8	0	27
78X-4, 120-122	641.43	11	0	6
80X-3, 137-139	658.79	7	0	6
83X-3, 57-59	687.26	9	0	6
164-995A-				
1H-1, 140-150	1.45	9	2	0
164-995B-				
1H-3, 108-118	4.08	17	2	0
1H-5, 140-150	7.40	48	1	0
164-995A-				
3H-1, 150-155	12.73	17	1	0
3H-6, 140-150	20.25	15	3	0
6H-6, 83-85	48.04	13	28	0
13H-5, 140-150	105.10	15	1	0
17H-5, 140-150	143.10	13	0	2
24X-1, 135-150	195.35	9	0	2
24X-1, 135-150	195.35	9	0	2
26X-1, 24-26	214.08	7	0	2
28X-3, 135-150	228.25	7	0	2
31X-2, 135-150	255.15	9	0	2
31X-6, 38-40	260.12	15	0	2
31X-6, 40-42	260.14	12	0	2
35X-3, 130-150	295.00	10	0	2
36P-1, 9-24	300.39	13	0	2
42X-1, 130-150	349.90	14	0	2
42X-3, 103-104	352.63	14	0	3
42X-3, 103-105	352.64	13	0	3
42X-3, 130-150	352.90	8	0	2
44X-1, 130-150	369.20	9	0	2
46X-3, 130-150	382.39	10	0	3
49X-4, 130-150	403.60	19	0	2
51X-2, 130-150	418.80	15	0	2
53X-1, 44-46	427.05	15	0	2
53X-1, 54-56	427.15	14	0	2
54X-2, 130-150	438.00	17	0	2
55X-1, 130-150	446.20	14	0	2
61X-6, 9-39	500.34	11	0	2
64X-4, 130-150	527.80	8	0	2
71X-4, 130-150	585.64	10	0	2
71X-6, 141-142	588.75	5	0	22
71X-6, 141-143	588.76	6	0	14
71X-6, 143-145	588.78	3	0	23
78X-1, 105-125	647.95	12	0	2
81X-5, 94-95	682.65	8	0	5
81X-5, 95-96	682.66	8	0	10
81X-5, 130-150	683.00	7	0	12
83X-5, 16-18	701.10	14	0	3
83X-7, 0-20	703.80	8	0	2
164-997A-				
5H-CC, 20-21	41.19	10	32	0
8H-3, 15-16	56.05	4	37	0
21X-2, 140-150	169.80	11	0	1
26X-2, 50-52	205.41	10	0	4
26X-2, 51-52	205.42	7	0	30
27X-1, 120-122	213.21	10	0	2
164-997B-				
2X-2, 49-50	330.10	19	0	3
2X-2, 51-52	330.11	12	1	16
8X-1, 70-72	443.71	12	0	3
8X-3, 141-143	447.42	13	0	3
20X-3, 125-150	543.45	11	0	2
23X-3, 120-121	562.60	7	0	9
23X-3, 120-122	562.61	7	0	4
33X-2, 109-111	638.06	8	1	6
33X-2, 110-111	638.07	14	1	16
46X-3, 119-120	734.43	18	0	2
46X-3, 120-121	734.44	6	0	26
47X-2, 44-46	743.04	10	0	3
47X-2, 45-46	743.05	10	0	5

depths below 100 mbsf, calcite remains a significant sediment component (≥10 wt%), dolomite abundance decreases to trace amounts, and disseminated authigenic siderite becomes a pervasive carbonate phase (~2–30 wt%). Each of these diagenetic zones will be discussed individually below.

Sulfate Reduction Zone (Upper 20 mbsf)

Calcite is the predominant carbonate phase within this part of the sedimentary section and is primarily biogenic in origin. Although small amounts of dolomite are present sporadically within this zone, their negative $\delta^{18}O$ values and the positive $\delta^{13}C$ values (Table 2; Figs. 5–6) suggest a detrital source. Increases in pore-water Sr^{2+} concentrations, and Sr/Ca and Mg/Ca ratios through this interval (Fig. 2) could be considered indicative of active carbonate diagenesis consistent with calcite dissolution and reprecipitation (Curtis and Coleman, 1986; Walter, 1986; Table 1). However, these linear pore-water profiles may also represent diffusion gradients between seawater and waters in an underlying "diagenetic zone" (e.g. below 20 mbsf). Sediment smear-slide observations; generally minor variations in mineralogy; calcite stable isotopic values indicative of equilibrium with seawater (rather than pore water); and distinct dolomite $\delta^{18}O$ values suggest that authigenic carbonates (at least in concentrations large enough to detect by routine measurements) are absent in the upper 20 m of the sedimentary section.

Sulfate/Methane Interface and Upper Methanogenic Zone

The negative $\delta^{13}C_{CaCO_3}$ values at, and directly below, ~20 mbsf (the sulfate/methane interface) suggests that significant carbonate precipitation commences at this level (Figs. 5, 8). Apparently, depletion of sulfate is enhanced by anaerobic methane oxidation (AMO) as methane generated at depth is consumed by reaction with sulfate at the sulfate/methane interface (Borowski et al., 1997; Borowski et al., Chap. 9, this volume). Because the isotopic signal of CH_4 is highly ^{13}C-depleted, the bicarbonate produced by the consumption of CH_4 through AMO will be ^{13}C-depleted as well. The production of interstitial bicarbonate (HCO_3^-) creates increased alkalinity at this interface, apparently creating an environment especially suited for carbonate precipitation (Fig. 9). Increased concentrations of DIC, decreased $Ca^{2+}$and Mg^{2+} concentrations (Fig. 5; and Paull, Matsumoto, Wallace, et al., 1996), and low $\delta^{13}C_{DIC}$ at the sulfate/methane interface supports the occurrence of active AMO and carbonate precipitation. Carbonate samples with negative $\delta^{13}C$ values also have heavier $\delta^{18}O$ values consistent with authigenic precipitation (Fig. 6).

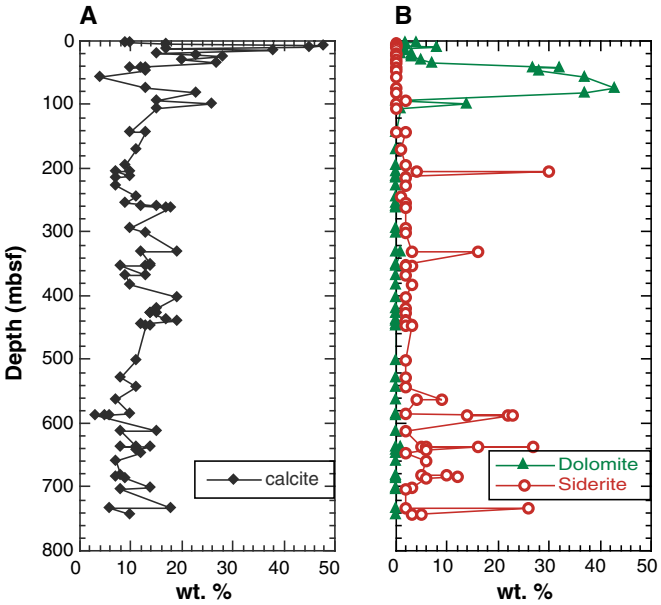

Figure 4. The distribution (in weight percent) of (**A**) calcite and (**B**) authigenic carbonate minerals (siderite and dolomite) are shown in sediments from Sites 994, 995, and 997. The corresponding data are shown in Table 3.

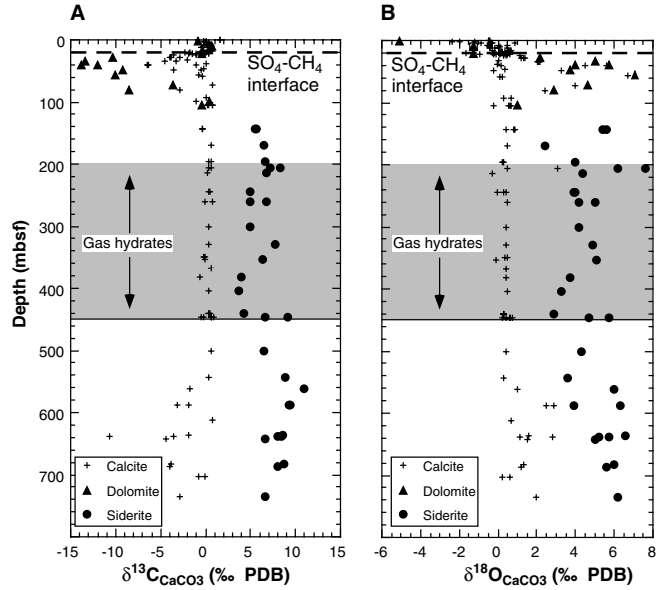

Figure 5. Variations in $\delta^{13}C$ (**A**) and $\delta^{18}O$ (**B**) of carbonate minerals (calcite, dolomite, and siderite) in sediments from Sites 994, 995, and 997 are shown. The corresponding data are given in Table 2. The sulfate/methane interface is indicated by a dashed line. The gas hydrate–bearing section of the sediment column is shaded.

Between 20 and 80 mbsf, authigenic dolomite occurs as discrete microcrystalline nodules in low abundance as disseminated rhombs within background sediment (Fig. 3B). Our pore-water profiles (Fig. 2) do not fit any single mechanism for dolomite formation (Table 1). This suggests that dolomite formation occurs by more than one mechanism in these sediments. The most common mechanism for dolomite formation (Table 1) in organic-rich continental margin settings is through replacement of pre-existing calcite (Baker and Burns, 1985). The minimal decreases in Ca^{2+} concentrations, combined with continued decreases in Mg^{2+} do suggest that dolomite has replaced

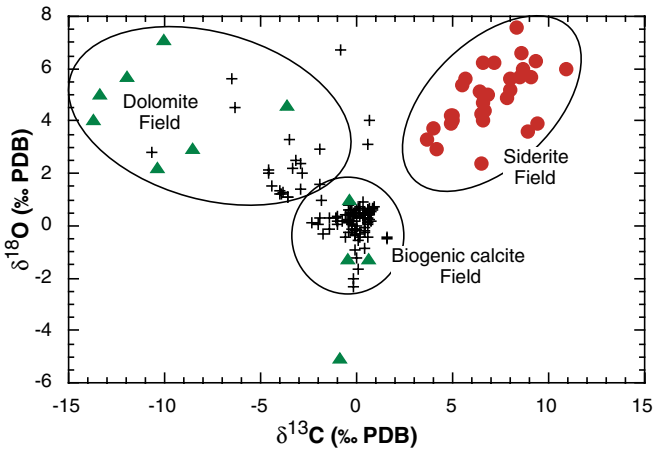

Figure 6. $\delta^{18}O$ and $\delta^{13}C$ cross plot for the same data as in Figure 5 and Table 2. Stable isotopic values for calcite, dolomite, and siderite are represented by crosses, triangles, and circles respectively. On the basis of their isotopic characteristics, carbonates from Sites 994, 995, and 997 are divided into three fields. (1) The Biogenic Calcite Field consists mostly of calcite with $\delta^{18}O$ and $\delta^{13}C$ values typical of biogenic calcite. (2) The Dolomite Field consists of authigenic dolomite (and some calcite), which exhibit depleted $\delta^{13}C$ and relatively heavy $\delta^{18}O$ values. (3) The Siderite Field is unique in that it consists solely of authigenic siderite with $\delta^{18}O$ and $\delta^{13}C$ values that exhibit no overlap with other carbonate phases in these sediments.

calcite ($CaCO_3 + Mg^{2+} + 2HCO_3^- \rightarrow CaMg(CO_3)_2 + CO_2 + H_2O$). However, the decrease in Mg/Ca and Sr/Ca ratios that would be required if dolomite was forming solely by the replacement of calcite is not observed. The observed increases in Sr/Ca ratios (Fig. 2) are also generally consistent with dolomite formation through direct precipitation from surrounding pore fluids (Table 1; $Ca^{2+} + Mg^{2+} + 4HCO_3^- \rightarrow CaMg(CO_3)_2 + 2CO_2 + 2H_2O$). The approximately 3:1 decrease in Mg^{2+}:Ca^{2+} that is observed on the Blake Ridge (Paull, Matsumoto, Wallace et al., 1996) suggests that dolomite forms by both direct precipitation from surrounding pore fluids, and by replacement of precursor calcite.

The extent to which calcite $\delta^{13}C$ values fall below a baseline established for typical pelagic carbonate $\delta^{13}C$ and $\delta^{18}O$ values reflects the contribution of authigenic carbonate to the total carbonate pool (Paull et al., 1992). Assuming that authigenic calcite formed near the present sulfate/methane interface has a $\delta^{13}C_{CaCO_3}$ value of –36‰, biogenic calcite has a $\delta^{13}C_{CaCO_3}$ value of 0‰, and there are no other contributors to the $\delta^{13}C_{CaCO_3}$ pool, then ~3%–20% of the calcite between 20 and 50 mbsf (corresponding with measured bulk $\delta^{13}C_{CaCO_3}$ values ranging from –1.0‰ to –7.3‰) was formed near this interface.

The addition of carbon derived from methane within the total carbonate pool is, in part, controlled by the rate at which anaerobic methane oxidation operates at the sulfate/methane interface and the extent of time methane oxidation is acting on a particular sedimentary horizon (Raiswell, 1988). Significant negative excursions in the $\delta^{13}C$ value of carbonates at depth may, therefore, reflect paleo sulfate/methane interfaces where AMO has been focused, leaving an enhanced ^{13}C-depleted signature on the bulk carbonate (Figs. 8B, 9).

The region of the sediment column where anaerobic methane oxidation takes place is associated with conditions that are optimal for carbonate precipitation (e.g., local increases in alkalinity). If sedimentation rates are high, the zone of optimal carbonate precipitation will move relatively rapidly upward through the sediment column. If the sedimentation rates slow, or there is a break in sedimentation, the sulfate/methane boundary will be stabilized at a particular level in the sediment column so that authigenic carbonate will be concentrated at, and just below, this horizon (Raiswell, 1988). Although there is no recognizable hiatus (based on lithologic or biostratigraphic evi-

dence), decreases in the sedimentation rate over the last 6 Ma have occurred on the Blake Ridge (Fig. 10; Paull, Matsumoto, Wallace, et al., 1996). This decrease has enhanced the likelihood that diagenetic carbonates produced at the sulfate/methane interface will be concentrated along a particular horizon (Raiswell, 1988; Hicks et al., 1996). The authigenic dolomite (and calcite), found within this region of the sediment column today, is a probable consequence of the recent decrease in sedimentation rates. Furthermore, the lack of authigenic calcite and dolomite at depths below 80 m, with isotopic signals suggestive of precipitation within this uppermost methanogenic zone, may be a consequence of the higher sedimentation rates during the Pliocene and Miocene.

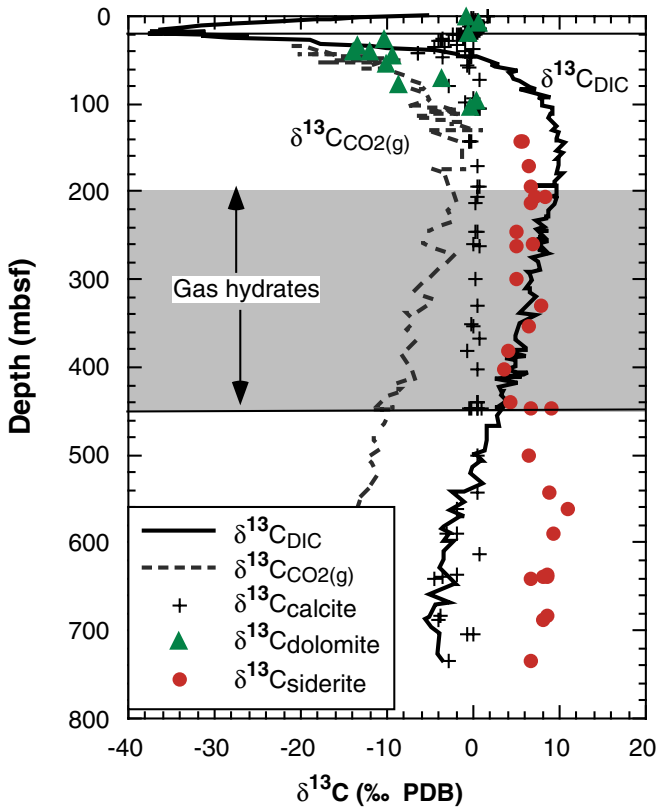

Figure 7. The $\delta^{13}C$ of carbonate minerals (calcite, dolomite, and siderite) are shown relative to the $\delta^{13}C$ of the DIC and $CO_{2(gas)}$ pools from Sites 994, 995, and 997 (solid line and dashed line respectively). The $\delta^{13}C$ of the DIC pool reaches a minimum at the sulfate/methane interface (SMI) and then increases to values as high as 10‰ PDB with depth. Below 200 mbsf, $\delta^{13}C$ of DIC decreases to values as low as –5‰ PDB. Authigenic siderite throughout the sedimentary section exhibits $\delta^{13}C$ values consistent with the DIC pool immediately above and within the gas hydrate–bearing section (shaded) of the sediment column.

Gas Hydrate Zone

The gas hydrate–bearing section of the sediment column, and the region immediately above, is characterized by high alkalinity (Fig. 2). In addition, whereas both Ca^{2+} and Mg^{2+} concentrations decrease sharply in the upper 40 m of the sediment column, Mg^{2+} concentrations and Mg/Ca values continue to decrease gradually through the gas hydrate zone (200–450 mbsf), suggesting continued active carbonate diagenesis (Fig. 2). The gradual decrease in Mg^{2+} through this zone is consistent with precipitation of nonstoichiometric siderite. Magnesium and, to a lesser extent, Ca commonly substitute for Fe in marine siderite (Mozley 1989). Furthermore, qualitative EDS analysis and previous studies of siderite from the Blake Ridge (Matsumoto, 1983, 1989) indicates that siderite in this sedimentary section contains both Mg and Ca (with a Fe:Mg:Ca ~ 6:3:1). Continued decreases in Mg/Ca ratios and sharp decreases in Sr/Ca ratios in the region between 100 and 250 mbsf (Fig. 2) suggest that the solutes required for siderite formation are derived from the surrounding pore fluids (Table 1). Between 200 and 450 mbsf (within the gas hydrate zone), a continued decrease in Mg/Ca, coupled with an increase in Sr/Ca ratios, may indicate that siderite formation is also occurring by replacement of precursor calcite (Table 1). However, we see no evidence (from smear-slide, thin section, and SEM observations) that siderite is replacing precursor calcite or dolomite (Table 1; Fig. 2). Moreover, siderite $\delta^{18}O$ and $\delta^{13}C$ values are tightly clustered (Fig. 6) and show no isotopic relationship with calcite or dolomite in this section.

It is unclear why the authigenic carbonate minerals change from dolomite to siderite downsection. There is no obvious lithologic change, nor abrupt change in total organic carbon (TOC; Paull, Matsumoto, Wallace, et al., 1996) between the dolomite- and siderite-bearing regions of the sediment column. Although there must be a source of iron for siderite to form, there does not seem to be a clear link between siderite and the minor amounts of pyrite (and/or trace occurrence of glauconite) contained within these sediments. Because clay minerals are the dominant lithologic component in much of the sedimentary section at Sites 994, 995, and 997 (Paull, Matsumoto, Wallace, et al., 1996), the source for Fe may be iron-oxide coatings on clay minerals and other terrigenous materials (Curtis and Coleman, 1986; Matsumoto, 1989; Hicks et al., 1996). The region of the

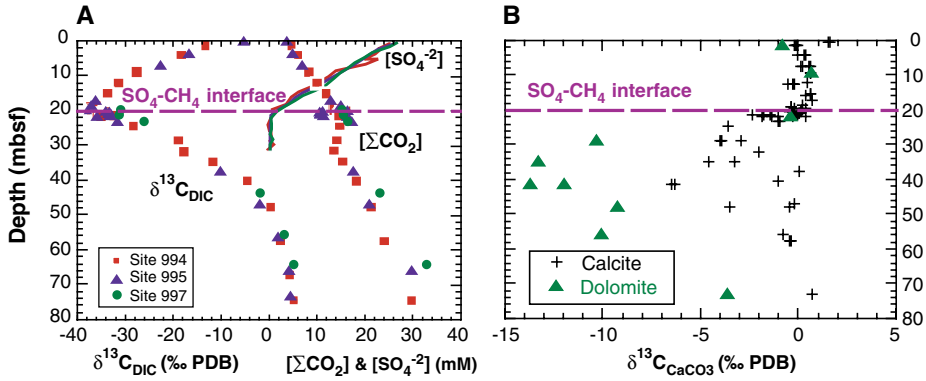

Figure 8. Expanded plots of the upper 80 m of the sedimentary section at Sites 994, 995, and 997 highlight (**A**) variations in pore-fluid concentrations of SO_4^{2-} and total dissolved carbon dioxide (ΣCO_2), and the $\delta^{13}C$ values of the dissolved inorganic carbon (DIC) pool; and (**B**) the $\delta^{13}C$ of carbonate minerals. The sulfate/methane interface marks a biogeochemical interface where methane (building up in sediments below) is consumed along with sulfate (diffusing downward from the seafloor) by microbially mediated anaerobic methane oxidation (AMO). The process of AMO produces conditions that are conducive to carbonate precipitation. Decreases in $\delta^{13}C$ values of both DIC and $CaCO_3$ at the SMI indicate that AMO is currently active.

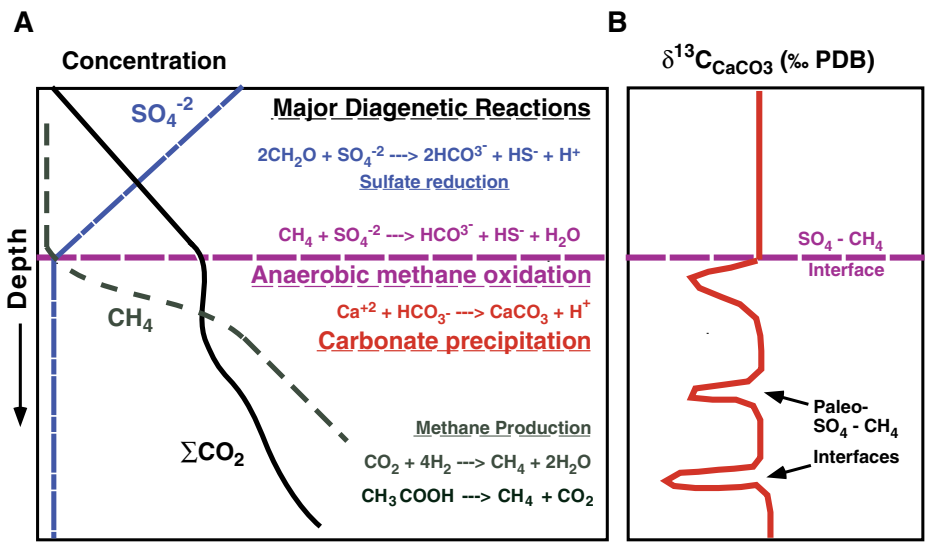

Figure 9. Drawing illustrating the major diagenetic reactions and possible response of authigenic carbonates is shown. **A.** The typical pore-fluid profiles produced by the major diagenetic reactions occurring in the upper part of marine sedimentary sections: (1) microbially mediated oxidation of organic matter by sulfate reduction, and (2) microbially mediated anaerobic methane oxidation (AMO). Both processes increase the alkalinity (by increasing DIC) of pore fluids and stimulate carbonate precipitation. **B.** Illustration of how the sedimentary record of carbonate minerals precipitated as a consequence of AMO will exhibit negative $\delta^{13}C$ values. Large negative excursions in the $\delta^{13}C$ value of carbonates at depth may reflect paleo sulfate/methane interfaces where AMO has been focused, leaving a ^{13}C-depleted signature on the bulk carbonate.

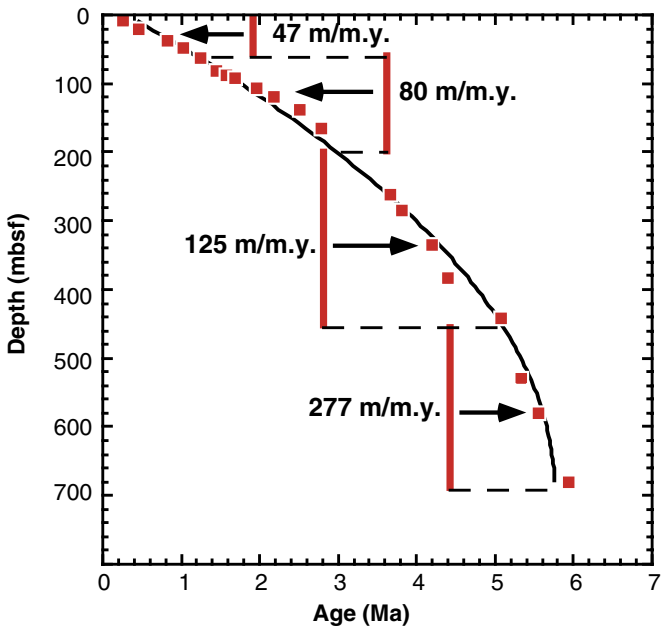

Figure 10. Changes in the sedimentation rate over the last 6 Ma at Site 994 are shown. Denoted age is based upon Shackleton et al. (1995). The Pleistocene decrease in sedimentation rate will enhance the likelihood that diagenetic carbonates will be concentrated along a particular horizon.

sediment column where siderite is present at the Blake Ridge is also coincident with the rapidly deposited sediments of the Pliocene and Miocene. Several authors have previously suggested that there may be an association between siderite occurrence and high rates of sedimentation (e.g. Berner, 1980; Curtis and Coleman, 1986; Mozley and Carothers, 1992; Mozley and Burns, 1993).

Authigenic siderite throughout these sedimentary sections exhibits $\delta^{13}C$ values that are reasonably consistent with the DIC (and CO_2 [gas]) pools between 120 and ~450 mbsf, which includes much of the gas hydrate–bearing zone (Fig. 7). The $\delta^{13}C$ of the DIC pool reaches a minimum at the sulfate/methane interface and then increases to a maximum between 120 and 150 mbsf, where values are as high as 10‰. The $\delta^{13}C$ values of CO_2 (gas) also parallel this trend (Fig. 7; Paull et al., Chap. 7, this volume). The $\delta^{13}C$ values of DIC decrease linearly below 150 mbsf to values as low as –5‰ (and $\delta^{13}C_{CO_2}$ of 18‰) at 750 mbsf. However, siderite values below ~450 mbsf do not match present-day $\delta^{13}C_{DIC}$ values. Furthermore, comparison of the ^{18}O values of siderite from Sites 994, 995, and 997 to calculated equilibrium values of $\delta^{18}O$ (Carothers et al., 1988) also indicate that siderite $\delta^{18}O$ values are approximately equivalent to the predicted equilibrium values immediately above and within the gas hydrate–bearing section of the sediment column (Fig. 11). The $\delta^{18}O$ values of siderite found deeper in the sedimentary section are inconsistent with precipitation beneath the gas hydrate–bearing section of the sediment column. Therefore, the positive $\delta^{13}C$ and $\delta^{18}O$ values of these siderites suggest that siderite formation on the Blake Ridge is linked to the high alkalinity associated with gas hydrates in these marine sediments.

CONCLUSIONS

Comparison between the distribution of carbonate minerals and pore-fluid chemistry in sediments associated with marine gas hydrates on the Blake Ridge, offshore of southeastern North America, reveals three distinct, depth-stratified, diagenetic zones.

1. The carbonates from the upper 20 mbsf (corresponding to the sulfate reduction zone) are primarily composed of calcite from biogenic sources and exhibit no evidence of diagenetic overprint.
2. Between 20 and 80 mbsf, authigenic dolomite with ^{13}C-depleted isotopic values becomes a dominant carbonate component.

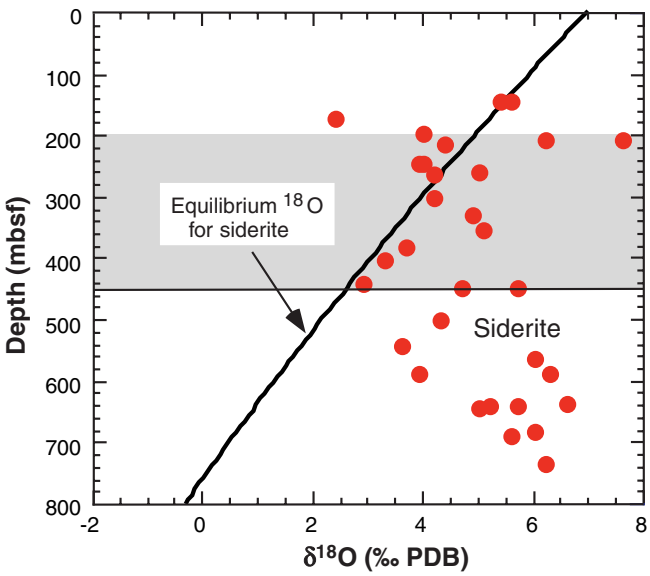

Figure 11. The $\delta^{18}O$ values of siderite samples from Sites 994, 995, and 997 are shown relative to the calculated equilibrium $\delta^{18}O$ values of siderite (solid line). This equilibrium line was calculated from the equation for fractionation between siderite and water (Carothers et al., 1988), assuming that the $\delta^{18}O$ of water is 0‰ PDB and that the geothermal gradient on the Blake Ridge is ~35°C/km (Ruppel, 1997). The $\delta^{18}O$ values of siderite found at depths greater than ~500 mbsf suggest formation shallower in the sediment column, where temperatures are cooler. Note that siderite $\delta^{18}O$ values have not been corrected for their phosphoric acid–liberated CO_2 fractionation (Carothers et al., 1988). The ~–1.4‰ shift for siderite that would result from applying a siderite acid–fractionation factor would still support our assertion that siderite formation occurs within, and above, the gas hydrate–bearing section of the sediment column on the Blake Ridge (120–450 mbsf).

Both dolomite and calcite precipitation is active within these sediments, especially near the sulfate/methane interface where anaerobic methane oxidation takes place.

3. Below 140 mbsf, siderite is ubiquitous and displays enriched $\delta^{13}C$ and $\delta^{18}O$ values that are consistent with the present-day isotopic values of the CO_2 and DIC pool, and with predicted equilibrium $\delta^{18}O$ values of siderite between 120 and 450 mbsf. These properties indicate that siderite forms above and within the gas hydrate–bearing section of the sediment column, where high alkalinity is conducive to carbonate precipitation.
4. Siderite found beneath the present-day gas hydrate zone is texturally and isotopically indistinguishable from siderite within the gas hydrate zone, and thus appears to be the buried remnants of early diagenesis. Siderite with enriched $\delta^{13}C$ values may, therefore, serve as a proxy for paleo gas hydrate–bearing sedimentary sections.

The distribution of carbonate minerals that we see today is not only reflective of currently active diagenesis, but also reflects how changes in sedimentation rates have affected diagenetic processes acting upon these sediments in the past. The presence of dolomite and calcite between 20 and 80 mbsf with isotopic signatures reflective of the uppermost methanogenic zone (where anaerobic methane oxidation and methane production by CO_2 reduction occur) may reflect decreases in sedimentation rates since the Pliocene. During the Miocene and Pliocene, high sedimentation rates prevented this "concentrated" zone of diagenesis from staying in place long enough to leave a "lasting" record of diagenesis.

ACKNOWLEDGMENTS

The authors would like to thank the ODP staff, A. Ribbens, and the crew of the *JOIDES Resolution*. We would also like to extend our gratitude to William Showers at North Carolina State University and Marshall Otter at Geochron Laboratories for assistance with stable isotope analysis. Steven J. Burns and John S. Compton provided a number of invaluable suggestions for improving this manuscript. This research was funded by a JOI/USSAC Ocean Drilling Fellowship to NMR.

REFERENCES

Al-Aasm, I.S., Taylor, B.E., and South, B., 1990. Stable isotope analysis of multiple carbonate samples using selective acid extraction. *Chem. Geol.,* 80:119–125.

Baker, P.A., and Burns, S.J., 1985. The occurrence and formation of dolomite in organic-rich continental margin sediments. *AAPG Bull.,* 69:1917–1930.

Berner, R.A., 1980. *Early Diagenesis: A Theoretical Approach:* Princeton, NJ (Princeton Univ. Press).

Blair, N.E., and Aller, R.C., 1995. Anaerobic methane oxidation on the Amazon Shelf. *Geochim. Cosmochim. Acta,* 59:3707–3715.

Borowski, W.S., Paull, C.K., and Ussler, W., III, 1997. Carbon cycling within the upper methanogenic zone of continental rise sediments: an example from the methane-rich sediments overlying the Blake Ridge gas hydrate deposits. *Mar. Chem.,* 57:299–311.

Burns, S.J., 1997. Early diagenesis in Amazon Fan sediments. *In* Flood, R.D., Piper, D.J.W., Klaus, A., and Peterson, L.C. (Eds.), *Proc. ODP, Sci. Results,* 155: College Station, TX (Ocean Drilling Problem), 497–504.

Carothers, W.W., Adami, L.H., and Rosenbauer, R.J., 1988. Experimental oxygen isotope fractionation between siderite-water and phosphoric acid-liberated CO_2-siderite. *Geochim. Cosmochim. Acta,* 52:2445–2450.

Claypool, G.E., and Kaplan, I.R., 1974. The origin and distribution of methane in marine sediments. *In* Kaplan, I.R. (Ed.), *Natural Gases in Marine Sediments:* New York (Plenum), 99–139.

Claypool, G.E., and Threlkeld, C.N., 1983. Anoxic diagenesis and methane generation in sediments of the Blake Outer Ridge, Deep Sea Drilling Project Site 533, Leg 76. *In* Sheridan, R.E., Gradstein, F.M., et al., *Init. Repts. DSDP,* 76: Washington (U.S. Govt. Printing Office), 391–402.

Compton, J.S., and Siever, R., 1986. Diffusion and mass balance of Mg during early dolomite formation, Monterey Formation. *Geochim. Cosmochim. Acta,* 50:125–135.

Curtis, C.D., and Coleman, M.L., 1986. Controls on the precipitation of early diagenetic calcite, dolomite, and siderite concretions in complex depositional sequences. *In* Gautier, D.L. (Ed.), *Roles of Organic Matter in Sediment Diagenesis.* Spec. Publ.—Soc. Econ. Paleontol. Mineral., 38:23–33.

Des Marais, D.J., 1978. Variable-temperature cryogenic trap for the separation of gas mixtures. *Anal. Chem.,* 50:1405–1406.

Dillon, W.P., and Paull, C.K., 1983. Marine gas hydrates, II. Geophysical evidence. *In* Cox, J.L. (Ed.), *Natural Gas Hydrates: Properties, Occurrences, and Recovery:* Woburn, MA (Butterworth), 73–90.

Gieskes, J.M., Gamo, T., and Brumsack, H., 1991. Chemical methods for interstitial water analysis aboard *JOIDES Resolution. ODP Tech. Note,* 15.

Hicks, K.S., Compton, J.S., McCracken, S., and Vecsei, A., 1996. Origin of diagenetic carbonate minerals recovered from the New Jersey continental slope. *In* Mountain, G.S., Miller, K.G., Blum, P., Poag, C.W., and Twichell, D.C. (Eds.), *Proc. ODP, Sci. Results,* 150: College Station, TX (Ocean Drilling Program), 311–323.

Hovland, M., Talbot, M.R., Qvale, H., Olaussen, S., and Aasberg, L., 1987. Methane-related carbonate cements in pockmarks of the North Sea. *J. Sediment. Petrol.,* 57:881–892.

Jorgensen, N.O., 1992. Methane-derived carbonate cementation of marine sediments from the Kattegat, Denmark: geochemical and geological evidence. *Mar. Geol.,* 103:1–13.

Kastner, M., Elderfield, H., Martin, J.B., Suess, E., Kvenvolden, K.A., and Garrison, R.E., 1990. Diagenesis and interstitial-water chemistry at the Peruvian continental margin—major constituents and strontium isotopes. *In* Suess, E., von Huene, R., et al., *Proc. ODP, Sci. Results,* 112: College Station, TX (Ocean Drilling Program), 413–440.

Klug, H.P., and Alexander, L.E., 1974. *X-ray Diffraction Procedures for Polycrystalline and Amorphous Materials:* New York (Wiley and Sons).

Lancelot, Y., and Ewing, J.I., 1972. Correlation of natural gas zonation and carbonate diagenesis in Tertiary sediments from the north-west Atlantic. *In* Hollister, C.D., Ewing, J.I., et al., *Init. Repts. DSDP,* 11: Washington (U.S. Govt. Printing Office), 791–799.

Land, L.S., 1980. The isotopic and trace element geochemistry of dolomite: the state of the art. *In* Zenger, D.H., Dunham, J.B., and Ethington, R.L. (Eds.), *Concepts and Models of Dolomitization.* Spec. Publ.—Soc. Econ. Paleontol. Mineral., 28:87–110.

Manheim, F.T., and Sayles, F.L., 1974. Composition and origin of interstitial waters of marine sediments, based on deep sea drill cores. *In* Goldberg, E.D. (Ed.), *The Sea* (Vol. 5): *Marine Chemistry: The Sedimentary Cycle:* New York (Wiley), 527–568.

Matsumoto, R., 1983. Mineralogy and geochemistry of carbonate diagenesis of the Pliocene and Pleistocene hemipelagic mud on the Blake Outer Ridge, Site 533, Leg 76. *In* Sheridan, R.E., Gradstein, F.M., et al., *Init. Repts. DSDP,* 76: Washington (U.S. Govt. Printing Office), 411–427.

————, 1989. Isotopically heavy oxygen-containing siderite derived from the decomposition of methane hydrate. *Geology,* 17:707–710.

Mozley, P.S., 1989. Relation between depositional environment and the elemental composition of early diagenetic siderite. *Geology,* 17:704–706.

Mozley, P.S., and Burns, S.J., 1993. Oxygen and carbon isotopic compositions of marine carbonate concretions: an overview. *J. Sediment. Petrol.,* 63:73–83.

Mozley, P.S., and Carothers, W.W., 1992. Elemental and isotopic compositions of siderite in the Kuparuk Formation, Alaska: effect of microbial activity and water/sediment interaction on early pore-water chemistry. *J. Sediment. Petrol.,* 62:681–692.

Paull, C.K., Chanton, J.P., Neumann, A.C., Coston, J.A., Martens, C.S., and Showers, W., 1992. Indicators of methane-derived carbonates and chemosynthetic organic carbon deposits: examples from the Florida Escarpment. *Palaios,* 7:361–375.

Paull, C.K., Matsumoto, R., Wallace, P.J., et al., 1996. *Proc. ODP, Init. Repts.,* 164: College Station, TX (Ocean Drilling Program).

Paull, C.K., Spiess, F.N., Ussler, W., III, and Borowski, W.A., 1995. Methane-rich plumes on the Carolina continental rise: associations with gas hydrates. *Geology,* 23:89–92.

Raiswell, R., 1988. Chemical model for the origin of minor limestone-shale cycles by anaerobic methane oxidation. *Geology,* 16:641–644.

Reeburgh, W.S., 1983. Rates of biogeochemical processes in anoxic sediments. *Annu. Rev. Earth Planet. Sci.,* 11:269–298.

Ritger, S., Carson, B., and Suess, E., 1987. Methane-derived authigenic carbonates formed by subduction-induced pore-water expulsion along the Oregon/Washington margin. *Geol. Soc. Am. Bull.,* 98:147–156.

Roberts, H.H., and Aharon, P., 1994. Hydrocarbon-derived carbonate buildups of the northern Gulf of Mexico continental slope: a review of submersible investigations. *Geo-Mar. Lett.,* 14:135–148.

Rosenbaum, J.M., and Sheppard, S.M.F., 1986. An isotopic study of siderite, dolomite and ankerite at high temperatures. *Geochim. Cosmochim. Acta,* 50:1147–1150.

Ruppel, C., 1997. Anomalously cold temperatures observed at the base of the gas hydrate stability zone on the U.S. Atlantic passive margin. *Geology,* 25:699–702.

Shackleton, N.J., Crowhurst, S., Hagelberg, T., Pisias, N.G., and Schneider, D.A., 1995. A new late Neogene time scale: application to Leg 138 sites. *In* Pisias, N.G., Mayer, L.A., Janecek, T.R., Palmer-Julson, A., and van Andel, T.H. (Eds.), *Proc. ODP, Sci. Results,* 138: College Station, TX (Ocean Drilling Program), 73–101.

Taylor, K.G., and Curtis, C.D., 1995. Stability and facies association of early diagenetic mineral assemblages: an example from a Jurassic ironstone-mudstone succession, UK. *J. Sediment. Petrol.,* A65:358–368.

Walter, L.M., 1986. Relative efficiency of carbonate dissolution and precipitation during diagenesis: a progress report on the role of solution chemistry. *In* Gautier, D.L. (Ed.), *Roles of Organic Matter in Sediment Diagenesis.* Spec. Publ.—Soc. Econ. Paleontol. Mineral., 38:1–11.

Date of initial receipt: 4 May 1998
Date of acceptance: 12 January 1999
Ms 164SR-227